Ultrasound in Med. & Biol., Vol. 47, No. 9, pp. 2664–2675, 2021

0301-5629/$ - see front matter

https://doi.org/10.1016/j.ultrasmedbio.2021.04.027

● *Original Contribution*

DESIGNED ANKYRIN REPEAT PROTEINS AS NOVEL BINDERS FOR ULTRASOUND MOLECULAR IMAGING

Alexandra Kosareva,* Mukesh Punjabi,* Amanda Ochoa-Espinosa,* Lifen Xu,* Jonas V. Schaefer,† Birgit Dreier,† Andreas Plückthun,† and Beat A. Kaufmann*,‡

* Cardiovascular Molecular Imaging, Department of Biomedicine, University of Basel, Basel, Switzerland; † Department of Biochemistry, University of Zurich, Zurich, Switzerland; and ‡ Department of Cardiology, University Hospital and University of Basel, Basel, Switzerland

(*Received* 8 *November* 2020; *revised* 7 *March* 2021; *in final form* 25 *April* 2021)

Abstract—Clinical translation of ultrasound molecular imaging will depend on the development of binders that can easily be generated, manufactured and coupled, and that are compatible with *in vivo* use. We describe targeted microbubbles (MBs) using designed ankyrin repeat proteins (DARPins) as a novel class of such translatable binders. Candidate DARPin binders for vascular cell adhesion molecule 1, an endothelial cell adhesion molecule involved in inflammatory processes, were selected using ribosome display and coupled to MBs. Flow-chamber assays of five MBs carrying high-affinity binders showed selective retention on endothelial cells activated by tumor necrosis factor-α for two binders compared with a MB carrying a control DARPin. *In vivo* ultrasound molecular imaging in a murine hind-limb inflammation model demonstrated up to a fourfold signal enhancement for three of the five MBs versus control. However, there was no correlation between results from flow-chamber assays and *in vivo* imaging. Thus, we conclude that ultrasound molecular imaging of inflammation using DARPin binders is feasible *per se*, but that screening of candidates cannot be accomplished with flow-chamber assays as used in our study. (E-mail: beat.kaufmann@usb.ch) © 2021 Published by Elsevier Inc. on behalf of World Federation for Ultrasound in Medicine & Biology.

Key Words: **Contrast ultrasound, Molecular imaging, Microbubbles, Designed ankyrin repeat proteins, Vascular cell adhesion molecule 1 (VCAM-1).**

INTRODUCTION

Contrast-enhanced ultrasound molecular imaging (CEUMI) has been developed to detect disease phenotypes at the cellular level (Kosareva et al. 2020), and thus allows for earlier detection of pathology, assessment of the effect of targeted therapies and tailoring of novel and expensive therapies to specific patients. CEUMI uses microbubbles (MBs) as contrast agents that are targeted to a specific disease-associated epitope by conjugating appropriate binders to the MB shell surface. It has been validated in animal models relevant for atherosclerosis (Kaufmann et al. 2007), myocardial ischemia (Davidson et al. 2012) and inflammation (Steinl et al. 2016), as well as in the detection of angiogenesis in tissue ischemia (Eisenbrey and Forsberg 2010) and neo-angiogenesis necessary for the growth of tumors (Deshpande et al. 2010).

Vascular cell adhesion molecule 1 (VCAM-1) is a cell adhesion molecule from the immunoglobulin superfamily, expressed on the endothelial surface upon appropriate inflammatory or angiogenic stimuli, and therefore is a potential target for molecular imaging in a number of clinical scenarios. VCAM-1 plays a role in the development of atherosclerosis by mediating the recruitment of monocytes to the vascular wall, and imaging of its expression could thus be used for early disease detection or risk stratification (Steinl and Kaufmann 2015). In chronic tissue ischemia, recruitment of monocytes that contribute to vasculogenesis by producing angiogenic peptides and adopting an endothelial phenotype is mediated by VCAM-1, and molecular imaging could thus be used to assess pro-angiogenic therapies in this context (Behm et al. 2008). In transplant rejection, VCAM-1 expression correlates with the degree of $CD3^+$ leukocyte infiltration and rejection, and consequently molecular

Address correspondence to: Beat A. Kaufmann, Department of Cardiology, University Hospital and University of Basel, Petersgraben 4, 4031 Basel, Switzerland. E-mail: beat.kaufmann@usb.ch

imaging could be used in place of invasive biopsies (Herskowitz et al. 1994). Furthermore, VCAM-1 is involved in tumor angiogenesis, and levels of endothelial expression of VCAM-1 correlate with tumor microvessel density, recurrence, metastasis and survival (Ding et al. 2003; Chen et al. 2011).

Altogether, there is a clinical need for non-invasive imaging of the expression of VCAM-1. CEUMI of VCAM-1 has been shown to be feasible in murine models of atherosclerosis, angiogenesis and tumor neoangiogenesis using full-size antibodies (Kaufmann et al. 2007; Behm et al. 2008; Chadderdon et al. 2014), nanobodies (Hernot et al. 2012; Punjabi et al. 2019) and small-peptide binders (Moccetti et al. 2018). However, all of these studies used binders that were not developed specifically for CEUMI, which relies on attachment of the contrast agent to a target under flow conditions with only milliseconds available for bond formation, and the need to withstand shear forces acting upon bound MBs. Designed ankyrin repeat proteins (DARPins) are alternative, multipurpose affinity reagents that recognize targets with exceptional specificity (Plückthun 2015). They are small, single-domain proteins (14−20 kDa) built from ankyrin repeat motifs. Large DARPin libraries can be used to select potential binders by ribosome display (Binz et al. 2003) and can subsequently be screened for binding to a particular target protein such as VCAM-1 under the relevant assay conditions. Given the large number of potential binders that can be generated from such libraries, it is desirable that *in vitro* methods be usable early on to identify those candidate binders that are expected to perform best under the relevant conditions *in vivo*. The purpose of the present study was therefore to select DARPin binders for the extracellular domain of VCAM-1 from a large DARPin library using ribosome display, assess whether *in vitro* testing is able to select candidate binders that will perform efficiently *in vivo* and assess whether non-invasive CEUMI of the expression of VCAM-1 is feasible using DARPin binders.

METHODS

Selection of candidate DARPin binders for VCAM-1

To generate DARPin binders against VCAM-1, the extracellular domain of VCAM-1 (custom-made Met1-Glu698, C-terminus carrying AVI tag and His tag, produced in HEK293 cells; Sino Biological, Beijing, China) was biotinylated (BirA500 kit, Avidity) and immobilized on MyOne Streptavidin T1 streptavidin-coated beads (Pierce, Waltham, MA, USA). Ribosome display selections were performed as described elsewhere (Dreier and Plückthun 2012) using a library of 10^{12} DARPin candidates. Selections were performed over four rounds with decreasing target concentration and increasing washing steps to enrich for binders with high affinities.

After four rounds of selection, the enriched pool was cloned into an *Escherichia coli* pQIq-based expression vector as fusion with an N-terminal $MRGSH_{8-}$ (Met-Arg-Gly-Ser-His8)- and a C-terminal. and a C-terminal FLAG tag. After transformation of *E. coli* XL1-Blue, 384 randomly selected single clones were expressed in small scale in a 96-well format and lysed by addition of B-PER Direct detergent plus lysozyme and nuclease (Pierce). These bacterial crude extracts of single DARPin clones were subsequently screened to identify potential binders.

Screening for high-affinity DARPin binders for VCAM-1

Homogeneous time-resolved fluorescence (HTRF) screening assays were performed to identify DARPins with the highest affinity for VCAM-1 from the 384 bacterial crude extracts containing candidate binders. In order to identify DARPins binding to epitopes accessible on the cell surface, cell-based flow-cytometry screening assays were also performed.

For HTRF, binding of the FLAG-tagged DARPins to streptavidin-immobilized biotinylated VCAM-1 was measured using fluorescence resonance energy transfer (donor: streptavidin-Tb, acceptor: anti-FLAG-d2; Cisbio, Codolet, France). Experiments were performed at room temperature in white 384-well OptiPlate plates (PerkinElmer, Waltham, MA, USA) using Tag-lite assay buffer (Cisbio) at a final volume of 20 μL per well. Signals were recorded after an incubation time of 30 min using a Varioskan LUX multimode microplate reader (Thermo Scientific, Waltham, MA, USA) with the following settings: delay time, 60 μs; integration time, 200 μs; measurement time, 1000 ms; dynamic range, automatic. HTRF ratios were obtained by dividing the acceptor signal (665 nm) by the donor signal (620 nm) and multiplying this value by 10,000 to derive the 665/620 ratio. The background signal was determined by using reagents in the absence of DARPins.

For flow cytometry, bEnd.3 murine endothelial cells (CRL-2299, ATCC, Manassas, VA, USA) at passage number 28 or 29 were stimulated with mouse rm tumor necrosis factor-α (TNF-α) for 18−20 h (10 ng/mL; #410-MT, R&D Systems, Minneapolis, MN, USA) to induce VCAM-1 expression. Fifty thousand cells were incubated either with the bacterial crude DARPin extracts (not normalized for concentrations), with a biotinylated monoclonal anti-VCAM-1 antibody (rat anti-mouse CD-106, clone 429, #553330, BD Pharmingen, San Diego, CA, USA) or with a biotinylated negative isotype control antibody (kappa isotype clone R35-95, #563047, BD Pharmingen) for 30 min at 4°C on a rocking table. The cells were subsequently washed three

times with cold Hanks' balanced salt solution (#14175, Thermo Fisher, Waltham, MA, USA) with 1% bovine serum albumin. The bound DARPins were detected by incubation with a fluorescein isothiocyanate-labeled anti-FLAG secondary antibody at a 1:100 dilution (anti-FLAG-M2-FITC, #F4049, Sigma Aldrich, Burlington, MA, USA), whereas the antibodies were detected using fluorescein isothiocyanate-labeled streptavidin (S205, Leinco Technology, St. Louis, MO, USA) for 30 min at 4°C on a rocking table. After three washing steps, the cells were resuspended in 100 μL/well of cold 1:2000 diluted viability dye Zombie NIR (#423105, BioLegend, San Diego, CA, USA) in phosphate-buffered saline (PBS) and incubated for 20 min at 4°C on the rocking table. Finally, the cells were washed three times with PBS, fixed with 4% formaldehyde in PBS (#50000, Alfa Aesar, Kandel, Germany) for 20 min at 4°C on a rocking table and washed three times with PBS. Flow-cytometry measurements were performed on a CytoFLEX (Beckman Coulter, Brea, CA, USA), and FlowJo (FlowJo LLC, Ashland, OR, USA) was used for analysis.

For a rough estimation of DARPin binder affinity by flow cytometry, cells labeled with a control antibody were measured first. With this measurement, a 90% exclusion gate was set, below which cells were considered non-specifically labeled. For all further measurements, cells with a fluorescence intensity above this threshold were counted as stained. Binding was then estimated as the percentage of events above this threshold relative to the total number of cells counted. Binders for VCAM-1 were selected using an arbitrary cutoff of at least 25% cells counted as stained. Experiments were performed in a first round at a 1:20 dilution of the crude bacterial extracts. In a second round, candidate binders which showed binding above the pre-defined cutoff at 1:20 dilution of crude extracts were re-examined at a 1:200 dilution.

DARPin binders selected from HTRF and flow cytometry were subsequently expressed in small scale and purified using a 96-well immobilized metal affinity chromatography column (HisPur Cobalt plates, #89969, Thermo Scientific).

Flow-cytometry analysis was repeated with the purified selected DARPins as already described at a known concentration of 800 pM. Median fluorescence intensity (MFI) was measured and normalized to the MFI of cells incubated with the isotype negative isotype control antibody. A threshold of 1.0 was used to further narrow the number of candidate binders.

To allow maleimide conjugation, new DARPin constructs of the selected candidate binders were cloned bearing a free and unique cysteine at their C-terminus. Subsequently, expression of these constructs was performed at a 200 mL scale. After induction with 1 mM isopropyl β-D-thiogalactopyranoside and incubation for 4 h, expression cultures were harvested by centrifugation for 10 min at 4000 rpm. Cell pellets were resuspended in PBS 400 mM NaCl, 10% glycerol, 5 mM 1,4-dithiothreitol (DTT; #3483-12-3, Sigma) and 20 mM imidazole adding Pierce Universal nuclease, and cells were lysed using sonication. DARPins were purified over a HisTrap fast-flow crude column (#GE17-5255-01, GE Healthcare, Chicago, IL, USA) and desalted over a HiTrap 26/10 desalting column (#GE17-0851-01, GE Healthcare) using an Äkta Pure L1 system (GE Healthcare). Purity was analyzed by sodium dodecyl sulfate−polyacrylamide gel electrophoresis and size exclusion chromatography.

Saturation binding assay of high-affinity DARPin binders for VCAM-1

We stimulated bEnd.3 murine endothelial cells with mouse rm TNF-α for 18−20 h (10 ng/mL; R&D Systems) to express VCAM-1. Cells were incubated with the candidate binders, with the E3_5 control DARPin (Binz et al. 2003), with the monoclonal anti-VCAM-1 antibody or with an isotype control antibody in increasing concentrations (50 pM−100 nM). Flow cytometry as already described was subsequently used to quantify ligand attachment to the bEnd.3 murine endothelial cells. The MFI of the samples was normalized to the MFI of the samples incubated with the isotype control antibody.

Contrast-agent preparation and characterization

MBs were manufactured by sonication of a decafluorobutane-saturated aqueous solution containing 1,2-distearoyl-*sn*-glycero-3-phosphocholine (2 mg/mL; #850365C, Avanti, Alabaster, AL, USA), polyoxyethylene (40) stearate (1 mg/mL; #P3440, Sigma) and 1,2-distearoyl-*sn*-glycero-3-phosphoethanolamine-maleimide (0.14 mg/mL; #PSB-301, Creative PEGWorks, Durham, NC, USA). Flotation-centrifugation was used to separate MBs from lipid molecules not integrated into the MB shell.

Before conjugation to the MBs, the monomeric state of the DARPins was ensured by reducing the C-terminal cysteine residues. A 1 M stock solution of DTT (Sigma) was prepared freshly in degassed water, and 1 μL of DTT stock solution was added to 1 mL reaction volume of the DARPin binders (approximately 3 mg/mL DARPins, buffered with 50 mM tris, 150 mM NaCl and 1 mM DTT, pH 8), vortexed and incubated for 1 h at 37°C. A desalting procedure was used to remove the excess DTT using PD-10 gravity-flow columns (GE Healthcare), which were equilibrated with freshly degassed PBS. DARPins bearing a C-terminal cysteine were conjugated to the maleimide on the MB surface by incubation for 2 h at room temperature with continuous shaking at 600 rpm to produce VCAM-1-targeted MB_{DARPin}

bearing one of the DARPin binders or the non-targeted E3_5 (MB_{E3_5}). Flotation-centrifugation was used to remove non-bound DARPins.

To determine the amount of DARPins necessary to saturate the maleimide binding sites on the surface of MBs, 1×10^8 MBs were incubated with different amounts of DARPins labeled with *N*-hydroxysuccinimide-fluorescein, also containing a C-terminal cysteine (0, 20, 40, 80, 100, 120, 150 and 200 μg), as described earlier. After three washing steps, the amount of fluorescence and thus DARPins present on the MB surface was measured using flow cytometry.

To determine the number of DARPins actually conjugated to the MB surface, quantitative fluorescence analysis was used after removal of unconjugated DARPins. For that purpose, 1×10^8 MBs were incubated with 120 μg of DARPins (five candidate binders and the E3_5 control DARPin) labeled with *N*-hydroxysuccinimide-fluorescein (#76608-16-7, Thermo Scientific) for 2 h, which was deemed in the saturation range. MB concentration and mean surface area were measured using a Multisizer 3 (Beckman Coulter). The MBs were then destroyed by applying pressure at 100 mm Hg. The amount of fluorescence was measured using a Gemini XPS fluorescence microplate reader (Molecular Devices, Sunnyvale, CA, USA). Comparison to a reference standard of known fluorescent DARPin concentration allowed for the calculation of DARPin density on the MB surface. All measurements were performed in triplicates.

Conjugation of the DARPins to maleimide on the MB surface was also verified visually. For this purpose, a DARPin clone was labeled with *N*-hydroxysuccinimide-Alexa Fluor 488 (A20000, Thermo Fisher). MBs were then incubated with the DARPin clone, and fluorescence on the MB surface was detected using microscopy (Eclipse Ti, Nikon, Tokyo, Japan).

Assessment of in vitro attachment of MBs to VCAM-1 under flow conditions

Parallel-plate flow-chamber studies (gasket thickness, 0.254 mm; channel width, 2.5 mm; 31-001, Glycotech Inc., Gaithersburg, MD, USA) were conducted to examine attachment properties of MBs carrying the selected DARPin candidates using flow cytometry. Cell culture dishes (35 × 10 mm; Corning, Corning, NY, USA) with bEnd.3 murine endothelial cells grown to confluence were used. At 4 h before measurement, the cells were induced with mouse recombinant TNF-α (50 ng/mL; R&D Systems) to express VCAM-1 and then placed in an inverted position on a microscope for video recording. A fluorescent dye (3,3′-dioctadecyloxacarbocyanine perchlorate, 0.1 mg/mL; #34215-57-1, Sigma Aldrich, Burlington, MA, USA) was included in the formulation of the MBs for efficient visualization of floating MBs. Fluorescently labeled MBs coupled to VCAM-binding DARPins or control DARPin (3×10^6/mL), suspended in cell culture medium (Dulbecco's modified Eagle's medium) at 37°C, were drawn through the flow chamber with a syringe pump (Genie Plus, Kent Scientific, Torrington, CT, USA) at a flow rate that would result in a shear stress of 2 or 4 dyn/cm^2, corresponding to physiological shear stress in venules, which are the main site of recruitment of inflammatory cells (Popel and Johnson 2005). The number of MBs attached to the cells was counted for 20 optical fields after 5 min of continuous flow using fluorescence microscopy digital recordings (BX51WI, Olympus Life Science, Tokyo, Japan, equipped with a charge-coupled device camera, 40 × magnification). Quantification was performed by an investigator unaware of which DARPin was coupled to the MBs.

In vivo *CEUMI*

All animal experiments were performed in accordance with Swiss federal legislation and approved by the Animal Care and Use Committee of the University Hospital of Basel and the ethics committee of the Veterinary Office of the Canton of Basel. We used 133 C57BL/6J male mice, ages 15−21 wk and maintained on standard laboratory diet, were used for CEUMI. Anesthesia was induced with 5% isoflurane; 1.5% was used for maintenance. We injected 250 ng of recombinant TNF-α (R&D Systems) in 100 μL of PBS into the adductor muscle of the mouse hind limb, which generally results in a significant increase in endothelial VCAM-1 expression in a time- and dose-dependent manner (Khanicheh et al. 2012). The mice were placed on a heating pad to keep the body temperature at 37°C. After 4 h, jugular vein cannulation was performed for administration of MBs. Ultrasound imaging (Acuson Sequoia c512, Siemens Medical Systems USA Inc., Mountain View, CA, USA) was performed with a high-frequency linear-array probe (15L8) held in place by a railed gantry system. The short axis of the adductor muscle of the injected mouse hind limb was imaged using power modulation and pulse inversion (Contrast Pulse Sequence) imaging at a centerline frequency of 7 MHz and a dynamic range of 50 dB at a mechanical index (MI) of 0.87. The gain settings were adjusted just below visible tissue speckles and held constant throughout the study. We injected 2×10^7 MBs carrying the VCAM-1-binding DARPins (MB_{DARPin}) as well as control MB_{E3_5} intravenously in random order while imaging was paused. After 8 min of circulation time, one image was acquired at an MI of 0.87 to assess the signal from stationary as well as circulating MBs. All MBs within the field of view were then destroyed with several (>10) image frames (MI 0.87) at a pulsing interval of 20 ms. Post-destruction image frames (MI 0.87, $n = 5$) representing circulating MBs only, were then acquired at a

pulsing interval of 10 s. Images were transferred to an off-line computer, and video intensities were log-linear converted. The signal from attached MBs alone was calculated by digitally subtracting the average signal of the post-destruction contrast frames from the signal of the first pre-destruction contrast frame (Lindner et al. 2001). The region of interest was determined from anatomic images of the hind limb acquired at the end of each imaging sequence using fundamental imaging at 14 MHz. Image analysis was performed by an investigator unaware MB species in the individual imaging sequences.

Immunohistology

It has been shown that injection of TNF-α leads to expression of VCAM-1 in skeletal muscle (Horie et al. 1997). Immunofluorescence staining was performed to qualitatively assess vascular expression of VCAM-1. Frozen hind-limb muscle sections were mounted on glass slides, fixed in 4% paraformaldehyde, blocked with 3% bovine serum albumin in 0.4% Triton X-100 solution and incubated overnight at 40°C with anti-VCAM-1 (ab134047, Abcam, Cambridge, UK) and α-smooth muscle actin (#I5381, Sigma) antibodies. Goat anti-rat Alexa Fluor 546 (#A11010, Invitrogen, CA, USA) and goat anti-mouse Alexa Fluor 488 (#A11001, Invitrogen) were added and incubated for 1 h at room temperature. Sections were mounted with RotiMount FluorCare mounting medium (Carl Roth, Karlsruhe, Germany) and imaged on a Nikon Ti2 microscope.

Statistical analysis

Data were analyzed with GraphPad Prism version 8.0d (GraphPad Software, Inc., La Jolla, CA, USA). Data points are expressed as mean ± standard error of the mean. For saturation binding curves, curve fitting was carried out by nonlinear regression using the saturation binding model $Y = B_{max} \times X/(K_d + X)$. For comparison of MB sizes, a *t*-test was used. For comparison of groups in the surface-density, flow-chamber and animal experiments, a Kruskal–Wallis test with Dunn's *post hoc* multiple-comparison test was used. Spearman correlation was used for assessing correlation between results from flow-chamber and animal experiments. Values of $p < 0.05$ were considered statistically significant (two-sided).

RESULTS

Screening for high-affinity DARPin binders for VCAM-1

With HTRF measurements, 19 binders were identified that showed a fluorescence signal for binding to VCAM-1 above background (Supplementary Fig. S1, online only). In parallel, after two rounds of flow-cytometry screening with increasing dilution of crude bacterial extracts (1:20 and 1:200), 21 potential binders for VCAM-1 were identified using an arbitrary cutoff of at least 25% cells counted as stained (Supplementary Fig. S2, online only). Of these 21 potential binders, 8 were also identified in the HTRF screening (Fig. 1), resulting in a total of 32 potential binders. After sequencing, 8 candidates were double transformants and 2 candidates were identical, and thus 23 unique single clones of potential VCAM-1 binders were identified.

After small-scale expression and purification of the 23 selected candidate binders, repetition of flow-cytometry analysis yielded 5 DARPin binders with staining of endothelial cells above the pre-defined threshold (clones 1731_F9, 1732_F8, 1730_E12, 1732_D1 and 1730_C7; Figs. 1 and 2a). The 5 DARPin binders selected contained either two (1730_E12, 1732_D1, 1730_C7) or 3 (1731_F9, 1732_F8) randomized internal repeats (Supplementary Fig. S3a, online only). On size exclusion chromatography, 4 DARPins were identified to be predominantly monomeric, not including 1730_C7 (Supplementary Fig. S3b, online only).

Saturation binding assay of high-affinity DARPin binders for VCAM-1

The five high-affinity DARPin binders identified in the screening process were further characterized using a saturation binding assay on cells. The results of these experiments are shown in Figure 2b. Saturation binding curves are similar for all DARPins; however, there are differences in B_{max} values, and higher saturation binding for 1731_F9 and 1732_F8 compared with 1730_E12, 1732_D1 and 1730_C7. This indicates that the binders recognize different epitopes, some of which are accessible in only a fraction of molecules. The shape of the curve is not consistent with the hypothesis that the plateau height might reflect affinities. Since the anti-VCAM-1 antibody is bivalent and detected with a different secondary reagent, it cannot be directly compared. The derived equilibrium dissociation constants and B_{max} values for all tested ligands and the anti-VCAM-1 antibody are shown in Table 1. The unselected control DARPin E3_5 showed no binding to the target at any concentration, consistent with VCAM-1-specific binding of the identified DARPins.

Characterization of MB contrast agents bearing DARPin ligands

Flow cytometry and fluorometry experiments were used to determine the amount of DARPin binder necessary to fully saturate the available maleimide binding sites on the MB surface after completion of the chemical reaction (2 h) and measure the amount of DARPins coupled to the MB surface. The mean diameter of MBs used for characterization was 2.17 ± 1.03 μm, and the mean concentration was 2.6×10^8 MBs/mL. Incubation of

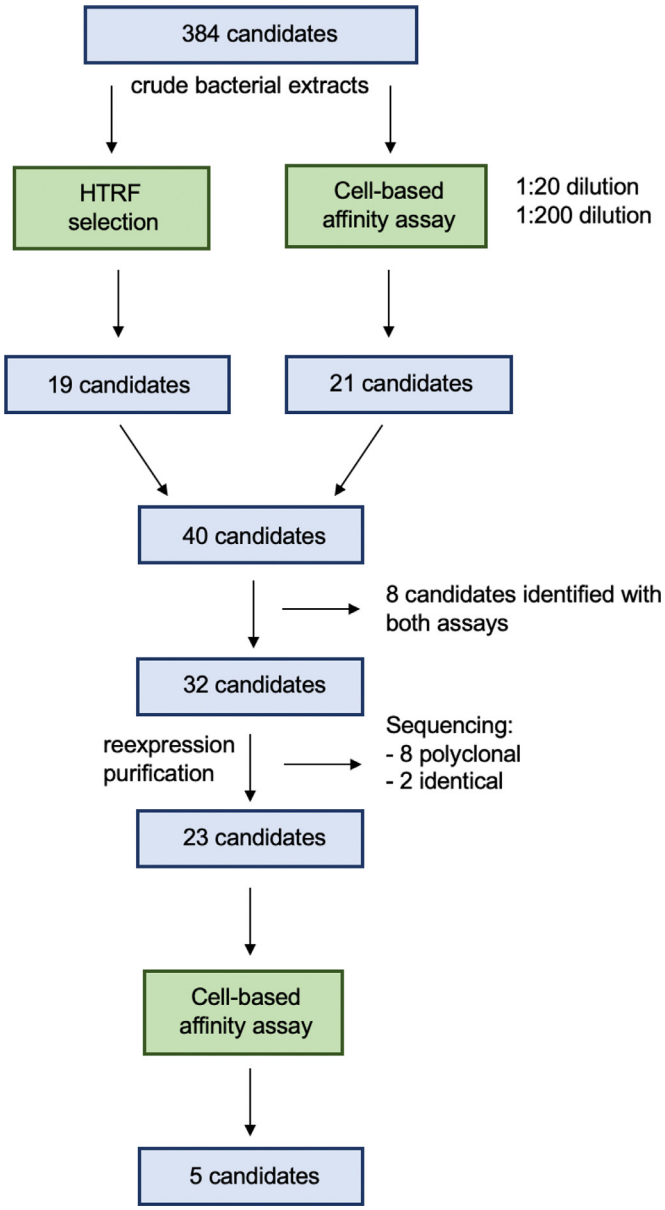

Fig. 1. Flowchart depicting the selection of five high-affinity binders from 384 candidate binders.

MBs with increasing concentrations of fluorescein-labeled DARPin showed that under these conditions, the coupling reaction becomes saturated at about 120 μg/ 1×10^8 MBs (Fig. 3a, 3b). Fluorescence microscopy revealed homogeneous staining of the MB shell with the DARPin clone 1731_F09 labeled with Alexa Fluor 488 (Fig. 3c). The number of DARPins per MB was determined as $1.5 \pm 0.2 \times 10^6$, and the average number of DARPin molecules per μm^2 as $6.4 \pm 1.4 \times 10^4$ (using the surface calculated from the measured diameter; Fig. 3d). When the measured surface densities were compared between the five candidate binders and the E3_5 control DARPin, there were no significant differences ($p = 0.74$, Fig. 3e).

Assessment of in vitro attachment of MBs to VCAM-1 under flow conditions

Flow-chamber studies at continuous flow were conducted, resulting in a shear stress of either 2 or 4 dyn/ cm^2. As shown in Figure 4a, there was a preferential retention of MB_{1730_E12} compared with the control MB_{E3_5} at 2 dyn/cm^2. The remaining MB_{DARPin} carrying the other four candidate binders showed some increased retention, which was, however, not significantly different

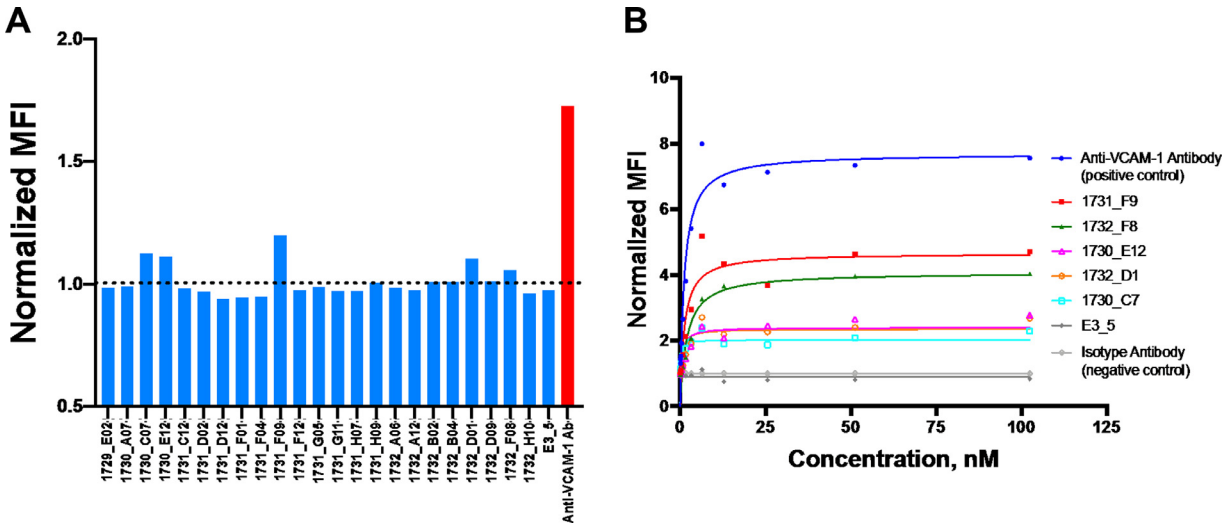

Fig. 2. (a) Binding comparison of 23 designed ankyrin repeat protein (DARPin) binders (*blue bars*) to vascular cell adhesion molecule 1 (VCAM-1) in the cell-based flow-cytometry assay. Purified DARPins were used at a concentration of 800 pM. The dotted horizontal line indicates the relative median fluorescence intensity of a non-binding isotype control antibody. Corresponding data for a bivalent anti-VCAM-1 antibody (*red bar*, detected by a different secondary antibody) are also shown. (b) Titration curves of individual DARPins and unselected control DARPin. Bivalent anti-VCAM-1 antibody and the corresponding isotype control antibody were used as positive and negative controls, respectively.

from that of MB_{E3_5}. However, at 4 dyn/cm^2 (Fig. 4b), the retention of MB_{1730_E12} was increased 10-fold over background, there was a fivefold increased retention of MB_{1732_D1} over MB_{E3_5}, and the remaining MB_{DARPin} carrying the other three candidate binders did not exhibit increased retention. Of note, the absolute magnitude of retention of MB_{1730_E12} was similar at both 2 and 4 dyn/cm^2, whereas the retention of MB_{DARPin} carrying all other candidate binders followed the same rank order at both stresses.

In vivo *CEUMI*

Vascular expression of VCAM-1 upon injection of TNF-α was verified using immunohistology (Fig. 5). MB preparations used for *in vivo* CEUMI had mean sizes of 2.39 ± 1.13 μm for VCAM-1-binding MB_{DARPin} and 2.46 ± 1.15 μm for MB_{E3_5} ($p = 0.87$); MB concentrations were 4.07×10^8 and 4.19×10^8 MBs/mL, respectively. Ultrasound molecular imaging of inflamed hind limbs showed significant fourfold increased signals for MB_{1732_F8} and MB_{1730_C7}, and a threefold increased signal for MB_{1732_D1} compared with MB_{E3_5}, whereas signals from MB_{1730_E12} and MB_{1731_F9} were not significantly different from MB_{E3_5} (Fig. 6). When the retention of the individual MB_{DARPin} in the flow chambers was compared with signal on ultrasound molecular imaging, there was no correlation between the two assays (Fig. 7; Spearman's $r = 0.49$, $p = 0.036$, and Spearman's $r = 0.31$, $p = 0.56$, for ultrasound molecular imaging of hind limbs vs. flow-chamber experiments at 2 and 4 dyn/cm^2, respectively).

Table 1. Saturation binding assay of high-affinity designed ankyrin repeat protein (DARPin) binders for vascular cell adhesion molecule 1 (VCAM-1) by flow cytometry, showing apparent equilibrium dissociation constants (K_d) and B_{max} values of the tested ligands

Ligand	K_d (M)	B_{max}
1731_F9 DARPin	1.19×10^{-9}	4.7
1732_F8 DARPin	1.92×10^{-9}	4.1
1730_E12 DARPin	0.40×10^{-9}	2.4
1732_D1 DARPin	0.33×10^{-9}	2.4
1730_C7 DARPin	0.11×10^{-9}	2.0
Anti-VCAM-1 antibody	1.18×10^{-9}	7.7

DISCUSSION

In this study, we describe the selection and *in vitro* as well as *in vivo* testing of DARPins binding to VCAM-1 as a novel class of binder molecules for use in ultrasound molecular imaging. From a large set of potential binders, five candidates were selected using a combination of HTRF and flow cytometry. These candidates showed similar apparent binding constants to VCAM-1 on cells, but their different B_{max} values may indicate binding to different epitopes with different accessibilities (Fig. 2b). Being equipped with a single cysteine at the C-terminus, a DARPin could successfully be coupled to the MB surface using maleimide chemistry. However, after binder attachment to MBs and under flow conditions in a

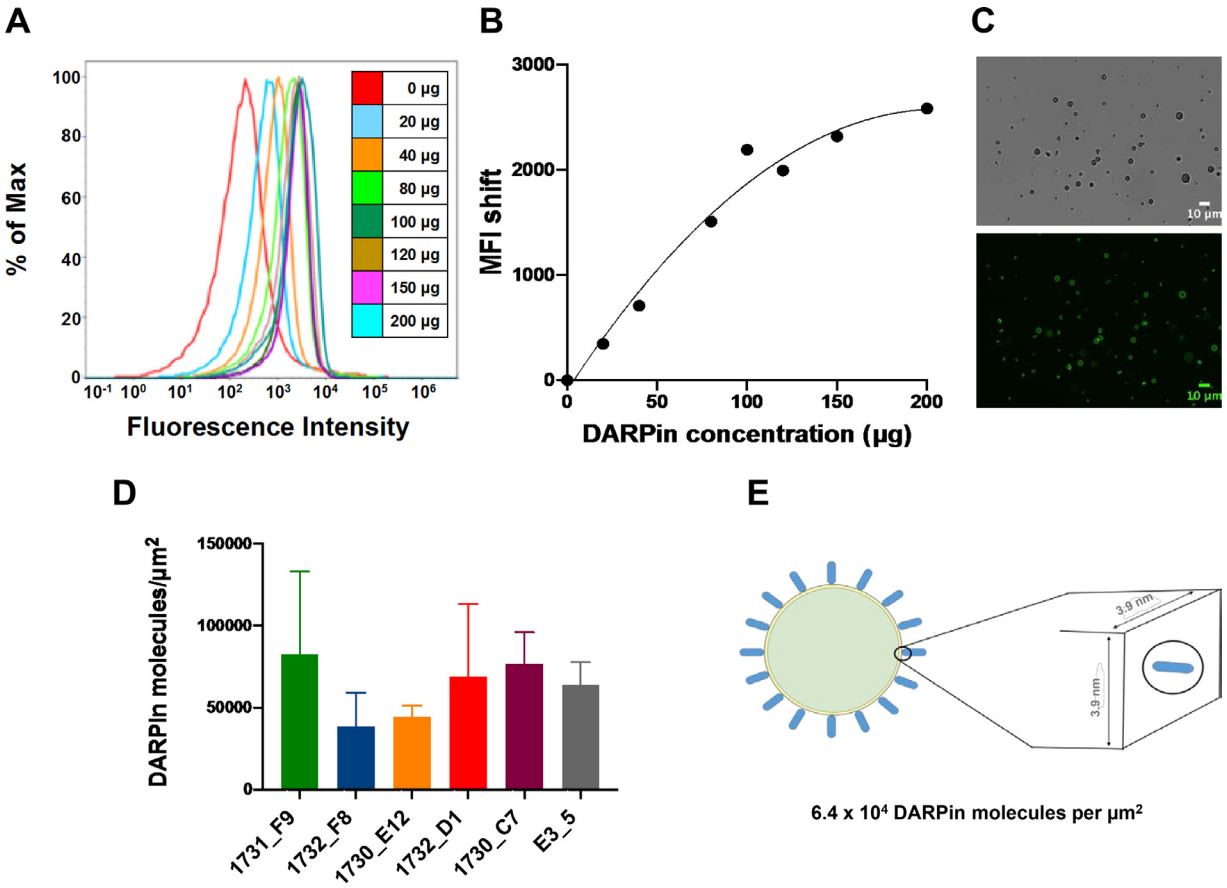

Fig. 3. (a) Determination of optimal conjugation amount of designed ankyrin repeat proteins (DARPins) by incubating 1×10^8 maleimide microbubbles (MBs) with increasing concentrations of fluorescently labeled cysteine-tagged DARPin 1730_E12 and measuring the fluorescence intensity of the MBs using flow cytometry. (b) Shift in median fluorescence intensity vs. baseline plotted against increasing concentrations of DARPin binder used for coupling. (c) Verification of conjugation of fluorescently labeled DARPins to the MB surface using fluorescence microscopy. Bright-field (*top*) and fluorescent (*bottom*) microscopy of maleimide MBs incubated with fluorescently labeled cysteine-containing DARPin 1731-F09. (d) Measurement of DARPin surface density on MBs ($n = 3-4$ per DARPin binder) using fluorescence spectroscopy ($p = 0.74$ between different DARPin binders). (e) Average surface density of DARPins on the MB ($6.4 \pm 1.2 \times 10^4$ DARPin molecules/μm^2).

flow-chamber assay, differences in binder-induced MB adherence to VCAM-1 became evident among the five candidates. In an *in vivo* model of microvascular inflammation, 3 of the 5 DARPin ligands allowed for selective signal enhancement. Thus, non-invasive imaging of VCAM-1 expression in the microcirculation is possible using MBs carrying DARPin binders. However, there was no obvious correlation between our *in vitro* assays and *in vivo* imaging in terms of the performance of the individual DARPins, indicating that our flow-chamber assays are probably not predictive for the performance of candidate binders in ultrasound molecular imaging.

Most previous ultrasound molecular imaging studies have used biotin molecules coupled to lipids in the MB shell and coupling via streptavidin for attachment of the targeting ligands to the MB surface (Kosareva et al. 2020). However, this coupling strategy will not be translatable into the clinical field, as there are concerns regarding binding of endogenous biotin and the immunogenicity of streptavidin (Kaul 2008). Therefore, in our study a cysteine was added to the five high-affinity DARPins at the C-terminus, which allowed for oriented coupling to the MB surface using covalent maleimide—-thiol coupling. This resulted in 6.4×10^4 DARPin molecules per μm^2 MB surface, which compares favorably to previous data on maleimide coupling of binders with a similar molecular weight (nanobodies, 1.3×10^4 molecules/μm^2; Punjabi et al. 2019) and to biotin—streptavidin binding of antibodies (3.7×10^3 molecules/μm^2; Khanicheh et al. 2012). This is relevant because binder density on the MB surface has been shown to influence attachment efficiency (Weller et al. 2002).

DARPins are composed of ankyrin repeat proteins and form a right-handed solenoid structure with a convex and a

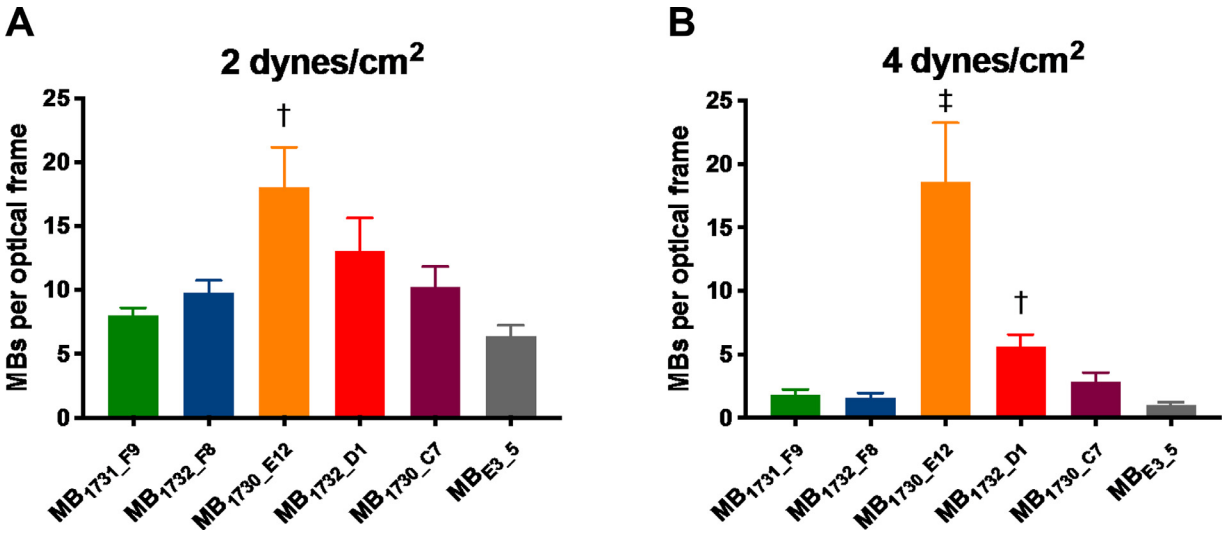

Fig. 4. Retention of MB_{DARPin} vs. control MB_{E3_5} in the *in vitro* flow-chamber assay at shear stresses of (a) 2 dyn/cm^2 and (b) 4 dyn/cm^2. †$p < 0.01$ vs. MB_{E3_5}; ‡$p < 0.0001$ vs. MB_{E3_5} ($n = 7–9$ per condition).

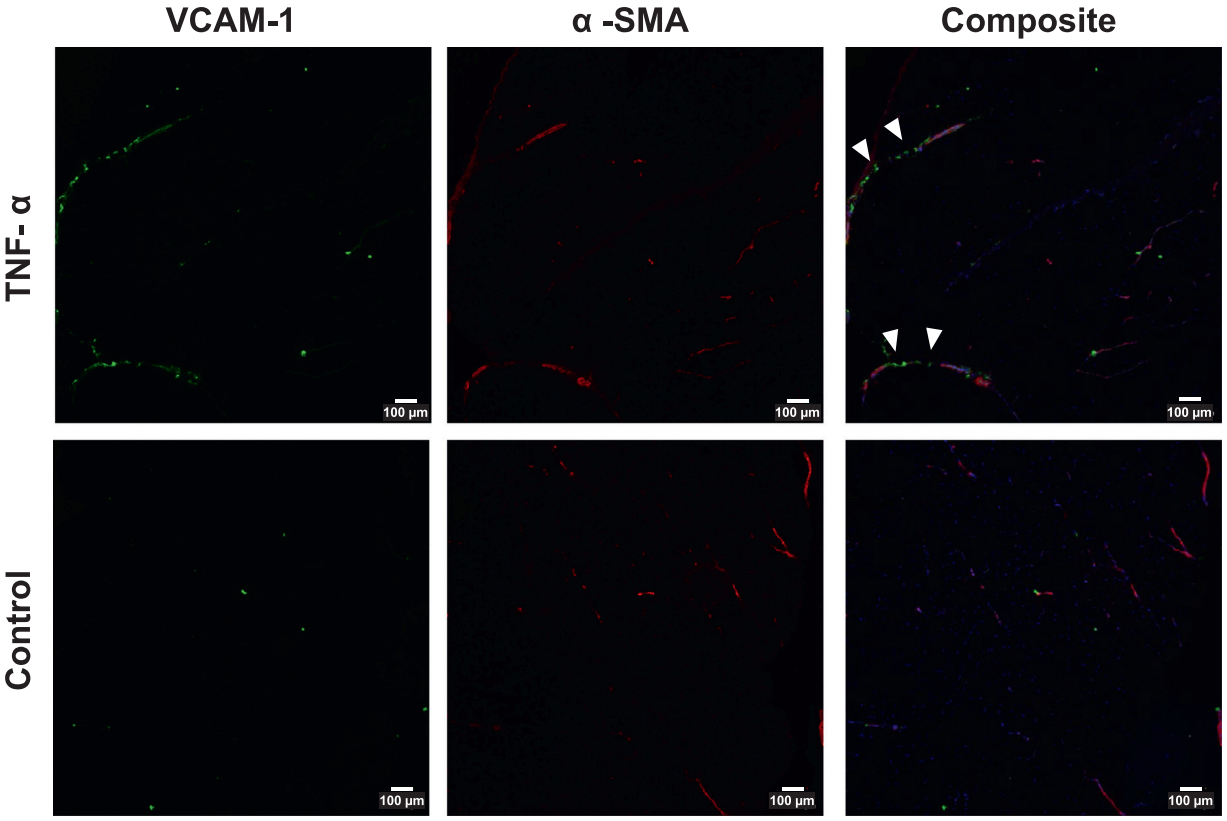

Fig. 5. Representative images of vascular cell adhesion molecule 1 immunofluorescence staining of the murine hind-limb muscle. (Top row) C57BL/6J male mouse (age 18 wk) injected in the hind limb with 250 ng tumor necrosis factor-α showing expression of vascular cell adhesion molecule 1 co-localized with blood vessels (identified by α-smooth muscle actin staining; *arrowheads*); (bottom row) control C57BL/6J male mouse (age 18 wk) showing no expression of vascular cell adhesion molecule 1 co-localized with blood vessels.

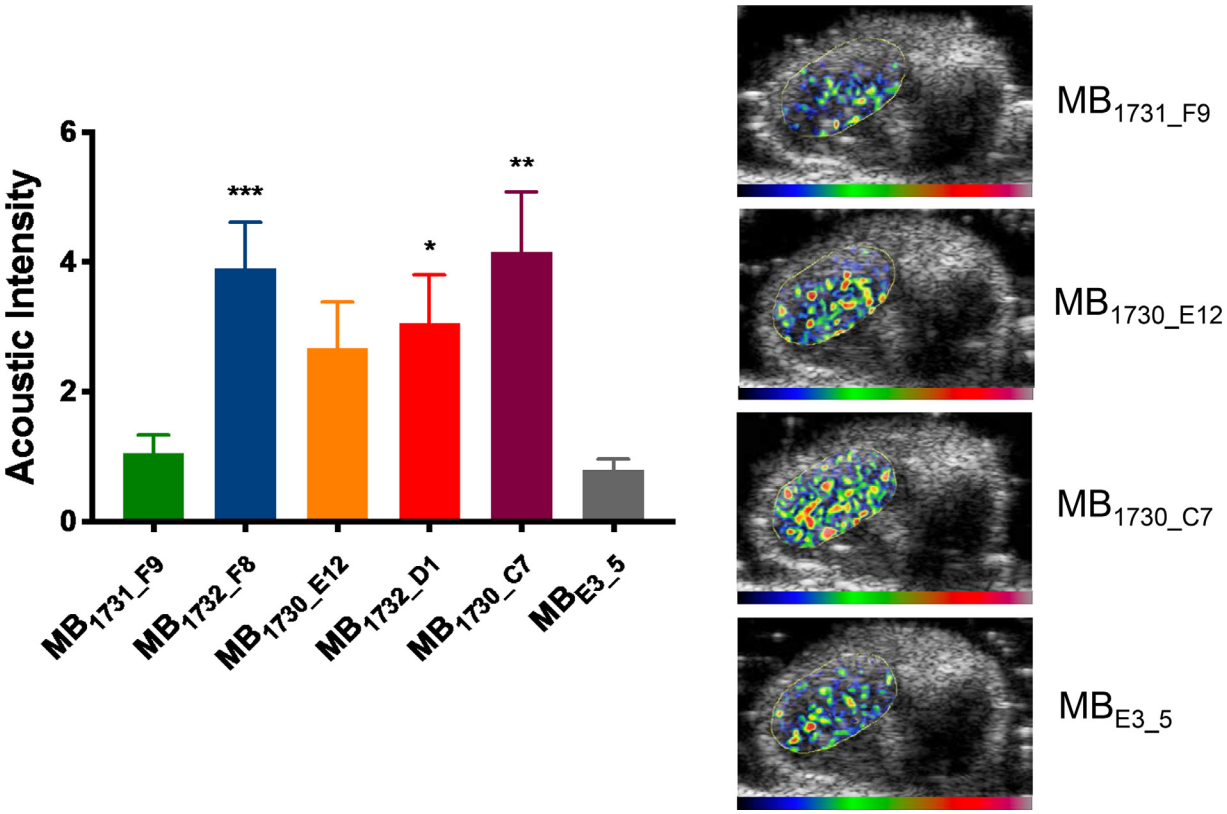

Fig. 6. Contrast-enhanced ultrasound molecular imaging of vascular cell adhesion molecule expression in hind-limb inflammation. In the right panels, examples of background-subtracted, color-coded contrast-enhanced ultrasound molecular imaging from one animal are shown. The color scale for the images is shown at the bottom of each frame. $*p < 0.05$, $**p < 0.005$, $***p < 0.0005$, vs. $MB_{DARPin\ control}$ ($n = 13$).

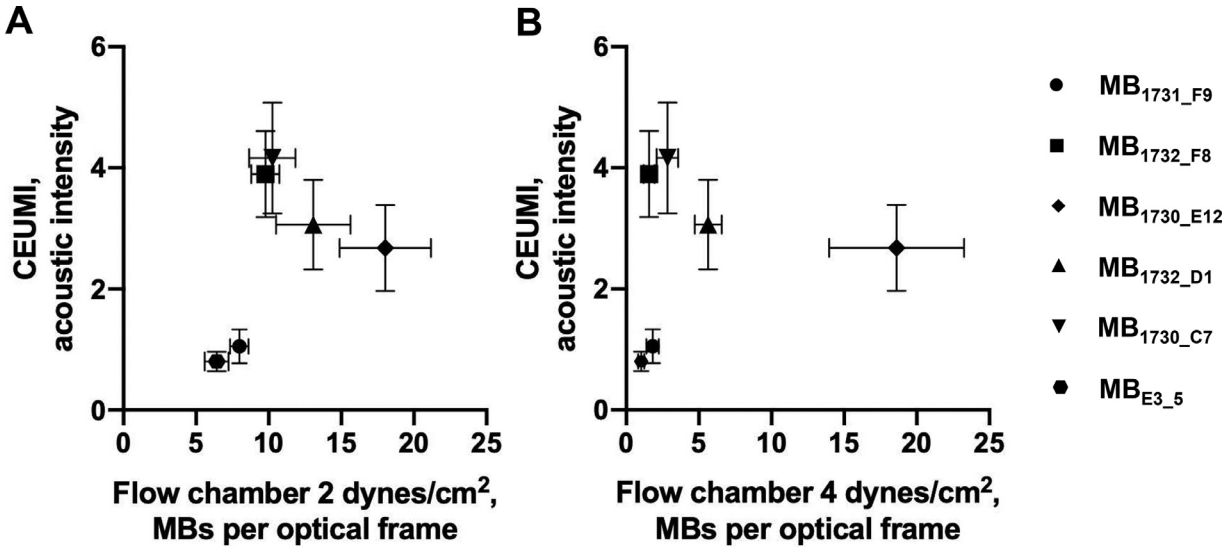

Fig. 7. Plots of signal intensities of $MB_{DARPins}$ vs. the results from the flow-chamber assay with those from hind-limb inflammation model for shear stresses of (a) 2 dyn/cm^2 and (b) 4 dyn/cm^2, illustrating the lack of correlation between these two assays.

concave surface. The groove on the concave surface serves as the binding site for target proteins (Plückthun 2015). The ligand−protein affinity is influenced by non-covalent interactions that depend on shape complementarity, interaction energy and electrostatic complementarity (Epa et al. 2013). Our saturation binding assay of the five DARPin candidates showed an apparent binding constant to VCAM-1 on cells in the low nanomolar range and only small differences between the individual DARPin binders, and the bivalent anti-VCAM-1 antibody performed similarly.

We used a parallel-plate flow-chamber assay for further characterization of MBs targeted to VCAM-1 with the five high-affinity binders, and noted considerable non-specific attachment of all MBs at a low shear stress of 2 dyn/cm^2, which was reduced at 4 dyn/cm^2, with prominent specific attachment of one MB carrying a high-affinity binder. Under laminar flow, endothelial cells undergo phenotypic changes, with actin fiber alignment parallel to the flow. Also, atomic force microscopy has been used to demonstrate small but significant increases in cell monolayer stiffness under laminar flow (Wong et al. 2016). The glycocalyx is a negatively charged polysaccharide brush on the surface of endothelial cells, ranging from 0.5−3 μm in thickness, with changes in thickness being induced by changes in shear stress (Calderon et al. 2011). We have previously shown that the thickness of the glycocalyx layer has an influence on targeted MB retention *in vivo* (Khanicheh et al. 2012). Thus, differences in endothelial phenotype caused by the different shear stresses may explain the different adhesion characteristics. When compared with experiments performed previously in our laboratory with an identical setup using either monoclonal antibodies or nanobodies targeted to VCAM-1, the attachment of MB_{1730_E12} was comparable to that of MBs carrying the antibody or nanobody ligands (Punjabi et al. 2019). Unexpectedly, the flow-chamber assays did not predict which DARPin binder would perform best *in vivo*. The differences in endothelial cell phenotype between the *in vitro* and *in vivo* setups may explain this.

On non-invasive ultrasound imaging in our model of TNF-α-induced hind-limb inflammation, three of the five DARPin binders tested showed increased signal compared with the control MB_{E3_5}, and two showed a robust fourfold increase in signal intensity. Of note, it has previously been shown that a decay of the targeted signal does not occur upon repeated injections of identical MBs targeted to an endothelial epitope (Streeter and Dayton 2013). Thus, ultrasound molecular imaging of the expression of VCAM-1 in the assessment of tumor vasculogenesis or angiogenic responses to ischemia is feasible. However, whether DARPin binders will also be feasible for the detection of VCAM-1 on endothelial cells in atherosclerosis will have to be studied in appropriate high-shear-stress settings.

There are several limitations of this study that deserve mentioning. First, we selected DARPin binders from a library of 10^{12} candidates, and randomly selected 384 hits for further characterization. Screening of a larger sample might have increased the probability of selecting more high-affinity binders, but most importantly, a stringent and extended affinity maturation could be used to improve the existing and additional binders. Also, the use of bivalent and bispecific formats engaging additional VCAM-1 epitopes may improve performance under high shear stress. With regard to high-throughput screening, surface plasmon resonance could possibly have given additional information regarding binding affinity in more quantitative terms than is possible by estimation of flow-cytometry titrations.

With regard to the use of the parallel-plate flow chamber, the results of these assays were not able to predict *in vivo* performance. In this respect, the use of either blood plasma or whole blood might yield *in vitro* results that correlate better with *in vivo* observations. However, with current flow-chamber assays relying on large fluid volumes, this is technically not feasible. With regard to the *in vivo* experiments, testing of six different MBs resulted in a relatively long duration of experiments, and it is possible that changes in hemodynamics over time may have influenced MB retention. However, we randomized the sequence of MB injection, and thus such an effect should not have influenced the overall results. Also, when analyzing imaging signals according to the sequence of injection, we did not find a significant increase from the first to the last injection ($p = 0.12$). Last, we examined the use of MBs targeting VCAM-1 using DARPin binders in a low-shear-stress environment. The performance of these novel ligands in high-shear-stress environments such as the detection of endothelial inflammatory activation in atherosclerosis will have to be examined in future studies.

CONCLUSION

In conclusion, in this study we describe DARPins as novel binders for ultrasound molecular imaging with targeted MBs, avoiding the use of antigenic proteins for coupling and achieving a very high density upon coupling. We demonstrate the feasibility of non-invasively detecting VCAM-1 expression in a model of hind-limb inflammation using these novel MBs. However, our results also suggest that there are several parameters that can be further optimized in future work, and more predictive *in vitro* screens of different binders for their *in vivo* performance need to be evaluated.

Acknowledgments—The authors would like to thank all current and former members of the High-Throughput Binder Selection facility at the Department of Biochemistry of the University of Zurich for their contribution to the establishment of the semi-automated ribosome display that resulted in the generation of the DARPin binders used, especially Thomas Reinberg, Sven Furler and Joana Marinho for assistance in the selection and screening of DARPin binders, and Anna-Lena Schinke and Imre Törö for DARPin expression and purification. The authors also would like to thank Samira Wyttenbach for assistance in immunohistology. B.A.K. is funded through grants from the Swiss National Science Foundation (SNF 310030_169905 and SNF 310030_197673) and from the Cardiovascular Research Foundation Basel.

Conflict of interest disclosure—A.P. is a co-founder of and shareholder in Molecular Partners AG, which is developing DARPins for therapeutic purposes. For the remaining authors, no conflicts of interest are declared.

SUPPLEMENTARY MATERIALS

Supplementary material associated with this article can be found in the online version at doi:10.1016/j.ultrasmedbio.2021.04.027.

REFERENCES

Behm CZ, Kaufmann BA, Carr C, Lankford M, Sanders JM, Rose CE, Kaul S, Lindner JR. Molecular imaging of endothelial vascular cell adhesion molecule-1 expression and inflammatory cell recruitment during vasculogenesis and ischemia-mediated arteriogenesis. Circulation 2008;117:2902–2911.

Binz HK, Stumpp MT, Forrer P, Amstutz P, Plückthun A. Designing repeat proteins: Well-expressed, soluble and stable proteins from combinatorial libraries of consensus ankyrin repeat proteins. J Mol Biol 2003;332:489–503.

Calderon AJ, Baig M, Pichette B, Muzykantov V, Muro S, Eckmann DM. Effect of glycocalyx on drug delivery carriers targeted to endothelial cells. Int J Transp Phenom 2011;12:63–75.

Chadderdon SM, Belcik JT, Bader L, Kirigiti MA, Peters DM, Kievit P, Grove KL, Lindner JR. Proinflammatory endothelial activation detected by molecular imaging in obese nonhuman primates coincides with onset of insulin resistance and progressively increases with duration of insulin resistance. Circulation 2014;129:471–478.

Chen Q, Zhang XH, Massague J. Macrophage binding to receptor VCAM-1 transmits survival signals in breast cancer cells that invade the lungs. Cancer Cell 2011;20:538–549.

Davidson BP, Kaufmann BA, Belcik JT, Xie A, Qi Y, Lindner JR. Detection of antecedent myocardial ischemia with multiselectin molecular imaging. J Am Coll Cardiol 2012;60:1690–1697.

Deshpande N, Pysz MA, Willmann JK. Molecular ultrasound assessment of tumor angiogenesis. Angiogenesis 2010;13:175–188.

Ding YB, Chen GY, Xia JG, Zang XW, Yang HY, Yang L. Association of VCAM-1 overexpression with oncogenesis, tumor angiogenesis and metastasis of gastric carcinoma. World J Gastroenterol 2003;9:1409–1414.

Dreier B, Plückthun A. Rapid selection of high-affinity binders using ribosome display. Methods Mol Biol 2012;805:261–286.

Eisenbrey JR, Forsberg F. Contrast-enhanced ultrasound for molecular imaging of angiogenesis. Eur J Nucl Med Mol Imaging 2010;37 (Suppl. 1):S138–S146.

Epa VC, Dolezal O, Doughty L, Xiao X, Jost C, Plückthun A, Adams TE. Structural model for the interaction of a designed ankyrin repeat protein with the human epidermal growth factor receptor 2. PLoS One 2013;8:e59163.

Hernot S, Unnikrishnan S, Du Z, Shevchenko T, Cosyns B, Broisat A, Toczek J, Caveliers V, Muyldermans S, Lahoutte T, Klibanov AL, Devoogdt N. Nanobody-coupled microbubbles as novel molecular tracer. J Control Release 2012;158:346–353.

Herskowitz A, Mayne AE, Willoughby SB, Kanter K, Ansari AA. Patterns of myocardial cell adhesion molecule expression in human endomyocardial biopsies after cardiac transplantation: Induced ICAM-1 and VCAM-1 related to implantation and rejection. Am J Pathol 1994;145:1082–1094.

Horie Y, Chervenak RP, Wolf R, Gerritsen ME, Anderson DC, Komatsu S, Granger DN. Lymphocytes mediate TNF-alpha-induced endothelial cell adhesion molecule expression: Studies on SCID and RAG-1 mutant mice. J Immunol 1997;159:5053–5062.

Kaufmann BA, Wei K, Lindner JR. Contrast echocardiography. Curr Probl Cardiol 2007;32:51–96.

Kaul S. Myocardial contrast echocardiography: A 25-year retrospective. Circulation 2008;118:291–308.

Khanicheh E, Mitterhuber M, Kinslechner K, Xu L, Lindner JR, Kaufmann BA. Factors affecting the endothelial retention of targeted microbubbles: Influence of microbubble shell design and cell surface projection of the endothelial target molecule. J Am Soc Echocardiogr 2012;25:460–466.

Kosareva A, Abou-Elkacem L, Chowdhury S, Lindner JR, Kaufmann BA. Seeing the invisible—Ultrasound molecular imaging. Ultrasound Med Biol 2020;46:479–497.

Lindner JR, Song J, Christiansen J, Klibanov AL, Xu F, Ley K. Ultrasound assessment of inflammation and renal tissue injury with microbubbles targeted to P-selectin. Circulation 2001;104: 2107–2112.

Moccetti F, Weinkauf CC, Davidson BP, Belcik JT, Marinelli ER, Unger E, Lindner JR. Ultrasound molecular imaging of atherosclerosis using small-peptide targeting ligands against endothelial markers of inflammation and oxidative stress. Ultrasound Med Biol 2018;44:1155–1163.

Plückthun A. Designed ankyrin repeat proteins (DARPins): Binding proteins for research, diagnostics, and therapy. Annu Rev Pharmacol Toxicol 2015;55:489–511.

Popel AS, Johnson PC. Microcirculation and hemorheology. Annu Rev Fluid Mech 2005;37:43–69.

Punjabi M, Xu L, Ochoa-Espinosa A, Kosareva A, Wolff T, Murtaja A, Broisat A, Devoogdt N, Kaufmann BA. Ultrasound molecular imaging of atherosclerosis with nanobodies: Translatable microbubble targeting murine and human VCAM (vascular cell adhesion molecule) 1. Arterioscler Thromb Vasc Biol 2019;39: 2520–2530.

Steinl DC, Kaufmann BA. Ultrasound imaging for risk assessment in atherosclerosis. Int J Mol Sci 2015;16:9749–9769.

Steinl DC, Xu L, Khanicheh E, Ellertsdottir E, Ochoa-Espinosa A, Mitterhuber M, Glatz K, Kuster GM, Kaufmann BA. Noninvasive contrast-enhanced ultrasound molecular imaging detects myocardial inflammatory response in autoimmune myocarditis. Circ Cardiovasc Imaging 2016;9. e004720.

Streeter JE, Dayton PA. An in vivo evaluation of the effect of repeated administration and clearance of targeted contrast agents on molecular imaging signal enhancement. Theranostics 2013;3:93–98.

Weller GE, Villanueva FS, Klibanov AL, Wagner WR. Modulating targeted adhesion of an ultrasound contrast agent to dysfunctional endothelium. Ann Biomed Eng 2002;30:1012–1019.

Wong AK, L.Lanos P, Boroda N, Rosenberg SR, Rabbany SY. A parallel-plate flow chamber for mechanical characterization of endothelial cells exposed to laminar shear stress. Cell Mol Bioeng 2016;9:127–138.